AUT Journal of Electrical Engineering
10.22060/EEJ.2026.24359.5691

Attention-Guided Dehazing: A New Architecture with Low-Level and Multi-Level Channel Attention

Hossein Noori[1], Mohammad Hossein Gholizadeh[2], Gholamreza Memarzadeh[3]

[1]Assistant Professor, Department of Electrical Engineering, Vali-e-Asr University of Rafsanjan, Rafsanjan, Iran
[2]Assistant Professor, Department of Electrical Engineering, Vali-e-Asr University of Rafsanjan, Rafsanjan, Iran
[3]Assistant Professor, Department of Electrical Engineering, Vali-e-Asr University of Rafsanjan, Rafsanjan, Iran

Abstract:

Single-image dehazing has become increasingly vital in recent years due to its foundational role in enhancing high-level vision tasks such as object detection, remote sensing, and autonomous driving. While numerous deep learning-based approaches have been proposed, many still fall short in fully preserving image details and capturing complex haze patterns. In this paper, a novel end-to-end architecture for single-image dehazing is presented that addresses key limitations of existing methods. The proposed network integrates two innovative modules: the Low-Level Feature Attention (LLFA) module, which emphasizes the retention of fine-grained details often lost in deeper layers, and the Multi-Level Channel Attention (MLCA) module, which dynamically fuses low- and high-level features to improve the network's representational capacity. By leveraging these complementary modules across multiple resolution scales, the architecture achieves more effective feature extraction and superior haze removal. Extensive experiments on both synthetic and real-world datasets demonstrate that our method consistently outperforms state-of-the-art algorithms in both qualitative visual clarity and quantitative evaluation metrics. The results confirm the robustness and efficiency of the proposed approach in producing clean, detail-rich dehazed images.

Keywords:

[1] The corresponding author is Hossein Noori with email address: h.noori@vru.ac.ir

Defogging/dehazing, feature attention, deep learning, channel attention, convolutional neural networks.

1. Introduction and Literature Review

Images captured in adverse weather conditions—such as when dust or water particles are suspended in the air—suffer from diminished visibility and reduced contrast. As a result, these images become unsuitable for advanced computer vision tasks, including remote sensing, target identification, navigation, and video surveillance. Consequently, mitigating haze effects through defogging or dehazing techniques has become a significant and expansive area of research [1], with numerous methodologies proposed to address this challenge.

Early image defogging methods often relied on supplementary data, such as multiple images captured under varying conditions, including different polarization [2], [3] or weather conditions [4], [5]. While effective, these approaches introduce increased complexity and cost due to the need for additional information. Consequently, many researchers have shifted their focus toward single image dehazing, which provides a more cost-effective solution, although with limited performance. Single image dehazing algorithms can be broadly categorized into three main groups: fusion-based methods, deep learning-based approaches, and prior-based techniques.

Fusion-based methods [6]-[13] integrate multiple enhanced versions of a single hazy image to improve clarity without incurring additional acquisition costs. While these methods show promise, they often face challenges in dark regions, where the effective combination of information becomes particularly difficult. Several fusion strategies have been proposed to address these limitations, including the fusion of white balancing and contrast enhancement [6], the combination of the dark channel prior method with adaptive histogram equalization [7], the fusion of gamma-corrected multi-scale Laplacian images [8], the integration of multiple images obtained using varying patch sizes [9], and the fusion of four gamma-corrected images with the output of color-preserving adaptive histogram equalization [10]. Authors [11] present an efficient feature-based fusion technique to enhance single foggy images at the transmission level. Additionally, a depth fusion approach for defogging has been suggested in [12]. In [13], the authors proposed an adaptive

exposure multi-fusion method, where three gamma-corrected images and an adaptive histogram equalized image are fused using a multi-scale Laplacian pyramid.

Prior-based methods offer a faster and more reliable solution to single-image dehazing [14]-[47]. These methods estimate the dehazed image based on reasonable assumptions (priors) and an atmospheric scattering model. While they significantly improve visibility, they may fail when the fundamental assumptions are not met. A major limitation of these approaches is their reliance on local image patches, typically $r \times r$ neighborhoods. Real-world scenes often have varying haze densities and object sizes, which fixed-size patches may not accurately capture, leading to artifacts or limitations in detail recovery.

In [14], the author assumed that transmission and surface shading are independent. Building upon this, the author in [15] assumes that pixels within small image patches display a one-dimensional distribution in RGB color space, utilizing color lines for dehazing. This algorithm is further extended to incorporate non-local patches in [16]. Additionally, the Color Attenuation Prior (CAP) introduced in [17] employs a linear model to estimate the depth map for image dehazing. The authors of [18] contend that haze-free images exhibit higher contrast than their hazy counterparts, seeking to maximize local image contrast. While the results are visually appealing, they may lack physical accuracy.

In [19], the authors supposed that most local patches in outdoor haze-free images contain pixels with very low intensities in at least one color channel, a concept known as the dark channel prior (DCP). Using dark channel, the transmission map can be computed. However, this computation may be affected by a blocking effect due to the local patch-based approach, defined as an $r \times r$ neighborhood, used to calculate the dark channel. To address this issue, a soft matting algorithm is proposed. It is important to note, however, that the soft matting algorithm requires significant computational resources. Subsequent algorithms in [20] to [37] aim to enhance the efficiency of the method presented in [19] by employing various smoothing techniques.

10.22060/EEJ.2026.24359.5691

In [20], the authors replaced the soft matting algorithm with morphological opening. While this leads to less implementation time but it results in a more halo effect. In [21], two defogged images were generated in both RGB and YCbCr color spaces and then averaged. The process involved calculating transmission maps for the R, G, B, and Y channels. To smooth these maps, a gradient derived from a Laplacian filter was subtracted, followed by a mean filter. This method can be computationally more expensive than techniques using a single color space. In [22], the authors replaced soft matting with morphological opening, followed by a guided filter [23].

The transmission map in [24] is derived from an improved airlight estimate, which is calculated as a weighted average of airlights obtained from dark and bright channel priors. In [25], the authors replaced the soft matting process with bilateral and adaptive median filters to refine the transmission map. The method proposed in [26] employs adaptive transmission map smoothing, but it is computationally more expensive compared to single-map methods. Although the Markov Random Field (MRF) approach in [27] provides enhanced transmission map estimation, it introduces higher computational complexity. To preserve edges during defogging, probability-weighted moments (PWM) are combined with DCP [28]. In comparison to [19], the method in [29] achieves better local consistency by integrating additional constraints into the dehazing optimization problem. This two-step optimization approach improves performance but at the expense of increased computational complexity.

In [30], fog density-based segmentation is utilized, with atmospheric light estimated by contrast maximization in each segment, followed by a total variation (TV) model to ensure edge preservation. The method in [31] dehazes images in the HSV color space using color correction and a multi-phase level set formulation. In [32], soft matting is replaced with a novel median filter and edge-preserving smoothing to minimize the halo effect. The method in [33] proposes two defogging algorithms: one for refining the transmission map based on color channel variations, and another for segmenting the image into sky and non-sky regions and defogging each region separately. High dynamic range fog removal is applied to the DCP in [34]. The dark channel is obtained by fusing two dark channels, calculated separately using a

median filter and color inversion [35]. The method in [36] uses DCP for low-frequency defogging and combines the result with high frequencies for final image restoration. Additionally, in [37], a new defogging algorithm is suggested for hyperspectral images.

The method of stretching the saturation component of foggy images is proposed in [38]. While this technique is efficient and yields visually appealing results, it has the potential to darken the overall image, particularly when applied to input images with bright pixels across all color channels. In a similar vein, [39] introduces the saturation line prior (SLP), which facilitates dehazing through the utilization of the derived lines.

A multi-channel convolutional multi-scale Retinex color restoration (MSRCR) based algorithm is proposed in [40]. This method employs guided filtering, Gaussian convolutions, MSRCR enhancement, and white balancing for defogging. However, it is complex and time-consuming. In [41], another method utilizing Retinex theory is proposed.

The algorithm proposed in [42] estimates airlight using a decision image combined with the dark channel prior. It further computes the transmission map by leveraging the YCbCr color space, the Multi-Scale Retinex with Color Restoration (MSRCR), and maximum and minimum filtering. Another defogging algorithm, introduced in [43] [44-47], employs adaptive Retinex theory, which achieves satisfactory results but at the expense of increased computational complexity and time consumption.

Deep learning has emerged as a leading approach for single-image dehazing [48]-[64], significantly enhancing image restoration. Convolutional Neural Networks (CNNs) are frequently employed to learn the mapping from hazy to dehazed images. The network proposed in [48] comprises four key steps: feature extraction, multi-scale mapping, local extremum detection, and nonlinear regression. This work introduces two innovative concepts: the use of Maxout layers and a novel activation function called the Bilinear Rectified Linear Unit (BReLU). The network efficiently approximates the transmission medium to recover dehazed images. In [49], the foggy image is processed through two networks. The first is a recurrent

10.22060/EEJ.2026.24359.5691

module, followed by an encoder-decoder that employs a visual attention mechanism. The second network, a Runge-Kutta module, identifies structures within the image. The results from these two modules are then integrated to produce the final output.

In [50], the authors approximate foggy images using Taylor expansion, substituting the Laplacian for traditional derivatives within the Taylor series. They employ T-Unet at the base of the pyramid to reconstruct the dehazed image. In [51], Kashiminder's law is reformulated, and a novel convolutional neural network (CNN) is proposed to approximate $K(x)$, representing a combination of the transmission medium and atmospheric scattered light. The authors in [52] utilize four distinct convolutions alongside a standard convolution to create Detail Enhancement Blocks (DEB). They introduce a novel content-guided attention mechanism to generate a channel-specific spatial importance map, and a new fusion block is proposed to combine various feature types.

In [53], a dual-branch network is proposed to independently estimate the transmission map and atmospheric light. The transmission map is estimated using a pyramid-densely connected encoder-decoder network, while the atmospheric light is determined using a U-Net. To further enhance the quality of the reconstructed image, a discriminator-based GAN is introduced. The GAN's loss function is combined with the dehazing loss to refine the estimation process by minimizing the discrepancy between the reconstructed image and the ground truth. In [54], a multi-guided bilateral learning framework is introduced for dehazing 4K-resolution images. This framework begins by extracting features from a reduced-resolution image, which are then processed by an affine bilateral grid. The grid applies multi-guided matrices across different color channels to identify high-resolution features. These features are subsequently fused using a feature fusion network to produce the final dehazed image. Meanwhile, FFA-Net [55] introduces a novel Feature Attention (FA) block, comprising a channel attention layer followed by a pixel attention layer. The authors [55] sequentially employ residual blocks and FA blocks, with the final feature fusion performed using the FA block to enhance the dehazing process.

The authors of [56] utilize smoothed dilated convolution layers to prevent gridding artefacts and employ a standard convolution layer as a gate to fuse features at different levels. They also incorporate residual blocks in the intermediate layers. Additionally, GridDehazeNet, proposed in [57], combines downsampling, upsampling, and residual blocks. In [58], the authors combine Generative Adversarial Networks (GANs) with enhancing blocks and residual blocks for enhanced dehazing performance. Authors [59] a CNN-based dehazing network incorporating a multiple attention fusion mechanism. The network extracts and fuses multi-scale features through a feature extraction network, followed by comprehensive dehazing at the channel, pixel, and spatial levels using the attention fusion module. The module integrates local and global residual structures, significantly improving training speed and generalization performance.

When evaluating state-of-the-art algorithms, we observed that many deep learning-based methods produce output images with noticeable blurring or residual fog. To tackle this issue, this paper introduces a novel network architecture specifically designed for image defogging. The proposed network leverages features from multiple levels and scales to achieve more effective haze or fog removal. A central innovation of this work is the development of a new module, the multi-level channel attention (MLCA) mechanism, which seamlessly integrates both low-level and high-level features. Additionally, the module incorporates a residual structure to address the challenge of gradient vanishing, further enhancing the network's performance.

As networks grow deeper, there is a tendency to overlook low-level features, which often contain critical information. To address this issue, we propose a low-level feature attention (LLFA) module that ensures these crucial features are preserved and utilized by the network. Additionally, we introduce a pyramid structure to capture multi-scale feature attention, enabling the network to process features at various resolutions. All the proposed modules are applied across different input resolutions to extract multi-scale and multi-level features. This comprehensive approach enhances the network's ability to produce clear, fog-free images, effectively overcoming the limitations of existing methods and improving the overall quality of defogged images.

Finally, the contributions of this paper are summarized as follows:

- Unlike existing state-of-the-art algorithms that do not simultaneously consider low- and high-level features, the proposed network is explicitly designed to integrate both feature levels concurrently.
- The proposed method fuses low- and high-level features across three different resolutions, enabling the model to capture relationships between spatially distant features.
- The method repeatedly integrates multi-level features to prevent the loss of low-level information in deeper layers of the network.
- The effectiveness of the proposed approach is evaluated using PSNR, SSIM, FADE, NIQE, AG, and implementation time, and the results are compared with those of several recent studies.

The remainder of this paper is organized as follows: Section 2 introduces the proposed architecture in detail. Section 3 presents the simulation results and provides a comparative analysis with several existing algorithms. Finally, Section 4 concludes the paper.

2. The proposed architecture

This paper proposes a novel architecture for single-image defogging. The proposed method operates in an end-to-end manner, taking a single foggy image as input and producing a defogged image as output. The architecture employs three distinct modules arranged in a nested structure. Specifically, a channel attention module is integrated within a multi-level feature attention module to enhance focus on features across all hierarchical levels. As demonstrated in prior work [10], foggy images predominantly retain information in low-frequency and low-level features. To address this, a low-level feature attention module is designed to prioritize such features. This module leverages multiple multi-level feature attention components to effectively combine both low- and high-level features, thereby improving feature selection. In the proposed framework, all modules are fed with multi-scale inputs, enabling the extraction of both low- and high-level features at varying scales. This multi-scale approach ensures robust feature representation, ultimately facilitating the reconstruction of a high-quality defogged image.

2-1- The network architecture

The architecture of the proposed network is illustrated in Fig. 1. As shown, the foggy or hazy image undergoes a downsampling process twice, with a factor of 2. In this paper, convolutional neural networks with a stride of 2 are utilized for downsampling the foggy or hazy image. The rationale behind this approach is that better features can be extracted from images at different resolutions. Subsequently, both the original and downsampled foggy images are input into a component of the network, low level feature attention (LLFA) module, to extract and combine both low and high level features. This means that the network first decreases the resolution of the foggy image. The original image and its reduced-resolution versions are then passed to the LLFA modules to extract relevant features for dehazing. Since the LLFA module preserves the spatial dimensions of the feature maps, the extracted features from this module are then upsampled using bilinear interpolation to ensure equal dimensions. The fully upsampled combined features from various resolutions, which now are in equal dimension, are added to enhance their discriminatory power. Finally, these features are processed through two convolutional layers to identify even higher-level features, along with a skip connection to mitigate the vanishing gradient problem.

The proposed architecture processes input data across multiple scales to capture both fine-grained details and broader contextual features. Initially, the input at different scales is fed into multiple LLFA modules, which are designed to extract both low- and high-level features. This enables the LLFA modules to identify and enhance important features at various scales. Each attention layer then focuses on specific aspects of the input in different scales to further refine these features. The outputs of these attention layers are subsequently integrated, allowing the model to leverage complementary information effectively. This approach results in a robust feature representation that combines high-resolution details with contextual insights. Finally, the extracted features are passed through two sequential convolution layers to generate the defogged image. Table 1 shows the hyper parameters of the overall network.

10.22060/EEJ.2026.24359.5691

To further clarify the architecture, the channel attention module is applied within the MLCA module after feature concatenation, as discussed in the following sections. Each LLFA module contains ten MLCA modules, and a total of three LLFA modules are used to extract features from the input foggy image at three different resolutions. These components are described in more detail in the subsequent sections.

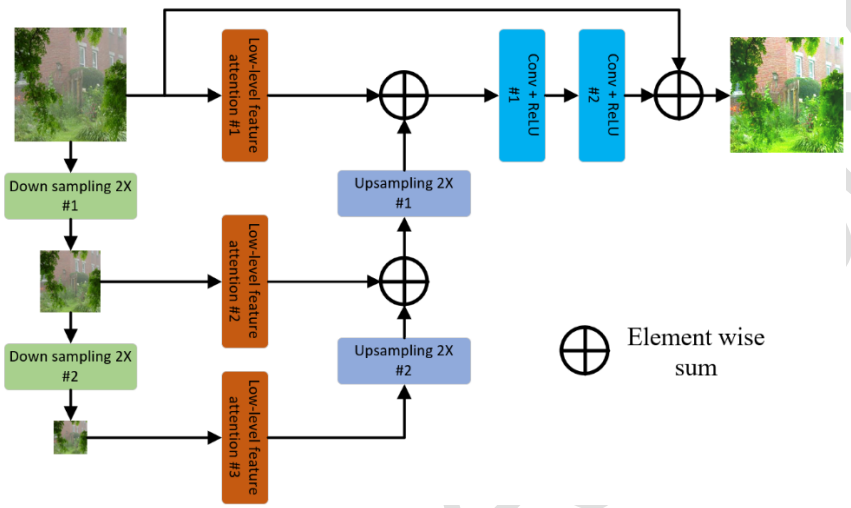

Figure 1: The proposed network architecture

Table 1. Hyperparameters of the proposed network

Layer	# of input channels	# of output channels	Size of input	Size of output
Down sampling #1	3	3	128×128	64×64
Down sampling #2	3	3	64×64	32×32
LLFA #1	3	3	128×128	128×128
LLFA #2	3	3	64×64	64×64
LLFA #3	3	3	32×32	32×32
Upsampling #1	3	3	64×64	128×128
Upsampling #2	3	3	32×32	64×64
Conv+ReLU #1	3	64	128×128	128×128
Conv+ReLU #2	64	3	128×128	128×128

2-2- Low level feature attention (LLFA) module

In previous methods, deep convolutional neural networks (CNNs) have been used to defog foggy images. However, as the network depth increases, low-level features are often ignored or forgotten. To address this issue, we propose a low-level feature attention (LLFA) module, a novel mechanism that enhances the network's ability to retain and utilize low-level features effectively.

The architecture of the LLFA module is illustrated in Fig.2. This module begins with a convolutional layer designed to increase the number of channels (feature maps), enabling the extraction of a broader range of features. Subsequently, multiple multi-level channel attention module (MLCA) —ten in this study—are employed to meticulously refine feature extraction. Another convolutional layer then restores the channel count to match the input dimensions. Finally, the input features are multiplied by the high-level features, mitigating gradient vanishing while enhancing the representation of hidden features within the lower-level feature space. The primary objective of the LLFA module is to identify and emphasize the most relevant features of the input. In this study, different resolutions of the input is fed to different LLFA to extract features in different resolutions. Consequently, high-level features from different resolutions are extracted and analyzed to improve the understanding and restoration of degraded visual content.

The proposed LLFA module leverages several (ten in this study) multi-level channel attention layers to enhance feature representation while maintaining essential information from the input data. Each attention layer operates by focusing on different scales of the input features, allowing the network to adaptively weigh the importance of various channels based on their relevance to the task. This hierarchical attention mechanism effectively captures both local and global dependencies, enabling robust learning from complex datasets. After processing through these attention layers, the original input is multiplied by the refined output, creating a rich composite representation that retains the foundational characteristics of the input while incorporating the transformational insights gained through attention. Table 2 shows the hyper

10.22060/EEJ.2026.24359.5691

parameters of the LLFA module. Note that in all the following Tables, the expression "same as branch" returns to the related resolution in Table 1.

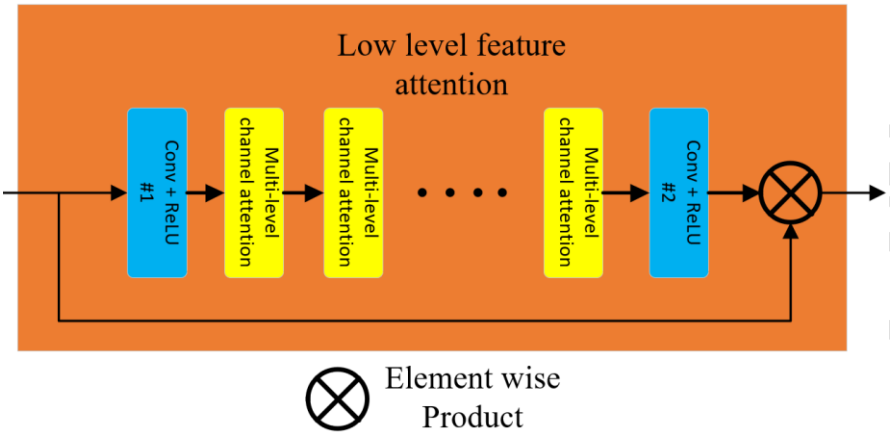

Figure 2: The low level feature attention (LLFA) block

Table 2: Hyperparameters of the low-level feature attention (LLFA) module

Layer	# of input channels	# of output channels	Size of input	Size of output
Conv+ReLU #1	3	4	Same as branch	Same as branch
MLCA	3	32	Same as branch	Same as branch
Conv+ReLU #2	32	3	Same as branch	Same as branch

2-3-Multi level channel attention (MLCA) module

Previous methods typically apply channel attention to the output of a single convolutional layer. In contrast, our proposed approach concatenates the outputs of multiple convolutional layers at different depths and then applies channel attention to the combined feature representation. This design ensures that if a lower-level feature is more salient than higher-level ones, it can still be preserved as the network deepens. Consequently, our method enables the joint consideration of multi-level features rather than focusing solely on higher-level representations.

10.22060/EEJ.2026.24359.5691

The proposed MLCA module, illustrated in Fig. 3, concatenates the outputs of three convolutional layers to effectively integrate both low- and high-level features. This design ensures a richer feature representation by preserving hierarchical information across different network depths.

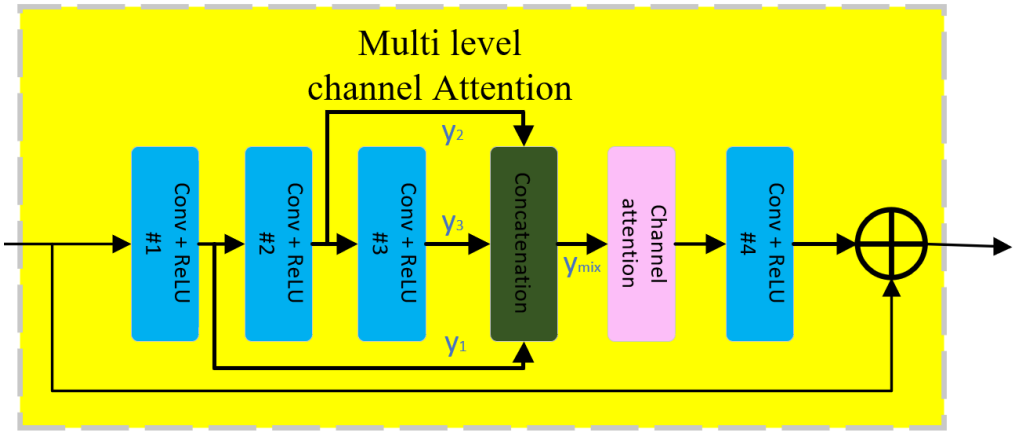

Figure 3: The multi level channel attention (MLCA) module

Table 3: Hyperparameters of the multi-level channel attention (MLCA) module

Layer	# of input channels	# of output channels	Size of input	Size of output
Conv+ReLU #1	3	8	Same as branch	Same as branch
Conv+ReLU #2	8	16	Same as branch	Same as branch
Conv+ReLU #3	16	32	Same as branch	Same as branch
Concatenation	(32,16,8)	56	Same as branch	Same as branch
Channel attention	56	56	Same as branch	Same as branch
Conv+ReLU #4	56	3	Same as branch	Same as branch

$$y_1 = R(conv(I)) \tag{1}$$

$$y_2 = R(conv(y_1)) \tag{2}$$

$$y_3 = R(conv(y_2)) \tag{3}$$

$$y_{mix} = concat(y_1, y_2, y_3) \tag{4}$$

10.22060/EEJ.2026.24359.5691

The concatenation layer, denoted as $concat$, stacks the outputs of convolution layers, namely y_1 (output of first convolution layer from left), y_2 (output of second convolution layer from left), and y_3 (output of third convolution layer from left) along the channel dimension. The input to the multi-channel attention module is represented as I . The concatenated features are then processed by a channel attention layer, which enhances feature selection by refining the representation of both low- and high-level features—this is the primary contribution of the layer.

Subsequently, a convolutional layer is applied to equalize the number of output channels with the input ones. To mitigate gradient vanishing, the module incorporates a residual connection, adding the input to the output. This final addition not only enriches the feature space but also improves performance in downstream tasks by preserving crucial information throughout the attention process. In this study, the LLFA module consists of ten MLCA layers.

$$OCA = CA(y_{mix}) \tag{5}$$

$$O_1 = R(conv(OCA)) \tag{6}$$

$$MLCA = I + O_1 \tag{7}$$

Where CA denotes the channel attention module (detailed in the next section), and OCA represents its output. I is the input to the MLCA module, while MLCA denotes the module's final output. Additionally, O_1 is an intermediate output. Table 3 shows the hyper parameters of the MLCA module.

2-4- Channel attention

Channel attention is an advanced mechanism in convolutional neural networks (CNNs) designed to enhance a model's ability to prioritize the most salient features across different channels. Each channel in a CNN typically represents distinct aspects of input data, such as color variations in images or syntactic structures in text. Channel attention operates by assigning adaptive weights to these channels based on their relevance

10.22060/EEJ.2026.24359.5691

to the specific task, enabling the network to amplify essential features while suppressing less informative ones. This process enhances feature representation, improving the model's ability to distinguish meaningful patterns from noise, ultimately leading to superior performance in tasks such as image recognition, segmentation, and object detection.

In image defogging, channel attention plays a critical role by emphasizing the distinct weighted information carried by different channel features, particularly in relation to DCP [19]. The process begins with the generation of a channel descriptor through global average pooling, which captures channel-wise spatial information. The extracted features are then processed using two convolutional layers to compute channel-wise weights [60]. Finally, the input channels are multiplied by these refined weights, ensuring effective feature enhancement and improved performance in image restoration tasks.

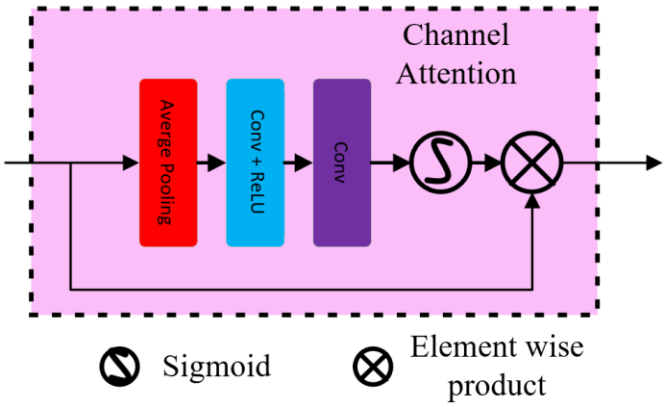

Figure 4: The channel attention block

Table 4: Hyperparameters of the channel attention module

Layer	# of input channels	# of output channels	Size of input	Size of output
Average pooling	56	1	Same as branch	Same as branch
Conv + ReLU	1	8	Same as branch	Same as branch
Conv	8	1	Same as branch	Same as branch

The architecture of the channel attention module is shown in Fig. 4. First a global average pooling is applied on each feature map (input channel).

10.22060/EEJ.2026.24359.5691

$$GAP^{c} = \frac{1}{H \times W} \sum_{i=1}^{H} \sum_{j=1}^{W} I^{c}(i, j) \tag{8}$$

Where $I^{c}(i, j)$ is the channel c of the input I, and i and j show the location of each pixel (row and column). Also, H and W show the total number of rows and columns of the input I. This layer changes the shape of input $C \times H \times W$ to the shape of output $C \times 1 \times 1$. Next a convolution layer followed by ReLU is applied to the output of feature maps. Then the outputs are processed by another convolution layer followed by a sigmoid activation function.

$$O_{ca_1} = S(conv(R(conv(GAP^{c})))) \tag{9}$$

where S shows sigmoid activation function. Finally, the input channels are multiplied by the extracted features.

$$O_{ca} = O_{ca_1} * GAP^{c} \tag{10}$$

It is necessary to mention that, applying channel attention mechanism to different scales of the input gives different feature maps which can be used in subsequent layers. As we know, to dehaze an image, transmission medium can be obtained with finding minimum of each channel in a local neighborhood, applying channel attention mechanism to different scales of input leads to find more important features, like transmission medium and atmospheric light, better. Table 4 shows the hyper parameters of the channel attention module.

To summarize, this paper introduces two feature extraction strategies: first, the network processes foggy images at multiple resolutions, and second, a feature attention mechanism is proposed to integrate low-level and high-level features for enhanced representation. The first approach aims to capture distinct, non-overlapping features, while the second adaptively combines complementary feature maps. This feature attention mechanism is realized through two novel modules: LLFA (Low-Level Feature Attention) and MLCA (Multi-Level Channel Attention). LLFA addresses the vanishing of low-level features in deeper

network layers, whereas MLCA effectively merges multi-depth features to prioritize more discriminative information.

3- Simulation results

In this section, the performance of the proposed algorithm is evaluated and compared against several state-of-the-art methods, including [17], [19], [38], [48], [52], [13], [20], [21], [35], [24], [18], [32], [10], [9], [61], [47], [41], [39], [62] and [63]. A comprehensive six-fold quantitative evaluation is conducted using three reference-based metrics—Structural Similarity Index (SSIM) [21], [64], Peak Signal-to-Noise Ratio (PSNR) [38], and Average Gradient (AG) [40]—alongside two no-reference metrics—FADE [65] and NIQE [66] [67, 68]—as well as the implementation time (see Table 5 for details). To further assess visual performance, a qualitative comparison is carried out using the original implementations of each referenced algorithm on selected test images. For consistency in timing evaluations, all methods are executed on the same hardware platform: a Lenovo Legion 7 laptop equipped with an Intel i7-10750H CPU, 32 GB of RAM, and an NVIDIA RTX 2070 Max-Q GPU.

Table 5: Definition of utilized criteria: I and J represent the foggy and defogged images, while μI and σI denote the average and variance of I. c1 and c2 are two constants, and rx represents the differential in the *x* direction. *M* and *N* correspond to the rows and columns of the image.

Criterion	Definition
PSNR	$PSNR = \frac{255}{\sqrt{\frac{1}{M \times N}\sum (J(x,y) - I(x,y))^2}}$
SSIM	$SSIM = \frac{(2\mu_I \mu_J + c_1)(2\sigma_{IJ} + c_2)}{(\mu_I^2 \mu_J^2 + c_1)(\sigma_I^2 \sigma_J^2 + c_2)}$
AG	$AG = \frac{1}{(M-1)(N-1)} \sum_{i=1}^{M-1} \sum_{j=1}^{N-1} \sqrt{(\nabla_x J(i,j))^2 + (\nabla_y J(i,j))^2}$

FADE	Refer to [65]
NIQE	Refer to [66]

3-1- Dataset and training setting

In this paper, the proposed method is trained and evaluated using both synthetic and real-world datasets. For the real dataset, we utilize the O-HAZE dataset from the NTIRE 2018 challenge. Specifically, from each 4K-resolution image, we extract fifty patches of size 128×128, resulting in a total of 2,250 paired hazy/clear image samples. For the synthetic dataset, we select 1,000 clear images from the Indoor CVPR09 dataset and another 1,000 from the Indoor Training Set (ITS) of the REalistic Single Image DEhazing (RESIDE) benchmark [68]. These images are resized to 128×128, and synthetic haze is applied. To simulate realistic haze, we vary the global atmospheric light between 0.8 and 1.0 and the scattering coefficient between 0.04 and 0.2. In total, 4,250 samples are used for training and evaluation: 4,000 for training and 250 for testing.

For training, the Adam optimizer is employed with its default parameters, $\beta_1 = 0.9$ and $\beta_2 = 0.999$. The initial learning rate is set to 0.001 and is halved every 1,000 training epochs. The proposed model is implemented using PyTorch and executed on a Tesla T4 GPU of Google Colab. The network is trained for a total of 6,000 epochs using the entire training dataset.

3-2- Quantitative comparison

This section presents a comparative analysis of the proposed method against several existing algorithms using six evaluation metrics: two reference-based criteria: SSIM and PSNR which assess similarity to ground truth images, and three no-reference criteria: AG, FADE and NIQE which provide an independent assessment of visual quality. Additionally, implementation time is evaluated to reflect practical and real-

time applicability. Higher values of PSNR, SSIM, and AG indicate more effective haze removal, whereas lower values of FADE, NIQE, and implementation time correspond to better performance.

Table 6 presents the average PSNR values comparing defogged images to ground truth across a set of 250 test images from both realistic and synthetic datasets. As shown in Table 6, the proposed method consistently achieves higher PSNR scores on the testing dataset, demonstrating its superior performance.

Table 6: Average PSNR between the original and defogged images on the 250 test images.

Algorithm	He [19]	Zhu [17]	Kim [38]	Cai [48]	Chen [52]	Li [62]	Proposed
PSNR	17.6239	19.6221	18.2274	20.3599	20.1824	19.0430	20.6151

Table 7 presents the SSIM values for the proposed method and competing algorithms. SSIM quantifies an algorithm's ability to retain structural information in an image, with values ranging from 0 to 1 (where 1 denotes identical images). Higher SSIM values generally indicate better preservation of image quality when a clear ground truth is available. As shown in Table 7, the proposed method achieves consistently higher SSIM values across the test dataset, demonstrating superior performance compared to traditional approaches.

Table 7: Average SSIM between the original and defogged images on the 250 test images

Algorithm	He [19]	Zhu [17]	Kim [38]	Cai [48]	Chen [52]	Li [62]	Proposed
SSIM	0.9524	0.8753	0.6494	0.9418	0.8374	0.6870	0.9679

Table 8 presents the AG values of the defogged images. As outlined in Table 5, higher AG values indicate greater image sharpness and richer detail content. Therefore, elevated AG scores reflect more effective preservation of image details during the defogging process. As shown in Table 8, the proposed method consistently achieves high AG values across both synthetic and real-world datasets, demonstrating its effectiveness in retaining fine image details throughout the defogging procedure.

The Fog Aware Density Evaluator (FADE) [65] is a widely adopted metric for assessing the real-world performance of image dehazing algorithms. Based on statistical analysis of a large dataset comprising both foggy and clear images, FADE serves two primary purposes: predicting scene visibility in foggy conditions and objectively evaluating the effectiveness of dehazing methods. Lower FADE scores indicate superior dehazing quality. As shown in Table 9, the method proposed in [38] achieves the lowest FADE value, followed by the approach in [17] and the proposed method, both of which outperform the remaining algorithms. Notably, the proposed method delivers the best performance among deep learning–based approaches, indicating its ability to extract more relevant features and make more effective use of them during the dehazing process.

Table 8: Average AG between the original and defogged images on the 250 test images.

Algorithm	He [19]	Zhu [17]	Kim [38]	Cai [48]	Chen [52]	Li [62]	Proposed
AG	62.0399	59.9256	79.2140	58.3951	51.8425	51.8606	60.3417

Table 9: Average FADE between the original and defogged images on the 250 test images.

Algorithm	He [19]	Zhu [17]	Kim [38]	Cai [48]	Chen [52]	Li [62]	Proposed
FADE	1.4454	1.1840	1.0841	1.4623	1.3410	1.3944	1.1841

Additionally, the quality of the results is assessed using the Natural Image Quality Evaluator (NIQE) [66], a reference-free metric that evaluates perceptual quality by comparing statistical features of defogged images to those of natural scenes. Lower NIQE scores indicate greater similarity to natural images, reflecting better perceived quality. As shown in Table 10, deep learning-based methods generally yield lower NIQE values, suggesting their superiority over other categories from a NIQE perspective. Furthermore, the proposed algorithm achieves lower NIQE scores across test datasets, indicating that it produces images statistically closer to natural scenes and potentially enhancing perceptual quality.

Table 10: Average NIQE between the original and defogged images on the 250 test images.

Algorithm	He [19]	Zhu [17]	Kim [38]	Cai [48]	Chen [52]	Li [62]	Proposed
NIQE	6.1410	6.5294	6.5895	6.1479	5.6932	5.7758	5.3482

Finally, Table 11 presents the execution time of the proposed algorithm in milliseconds. Notably, for deep learning-based algorithms, only prediction time is reported—training time is excluded. However, due to their dependence on computationally intensive operations, inference speed remains a critical consideration. As shown in Table 11, the algorithm from [17] achieves the fastest execution time, attributed to its use of a single linear equation per foggy image. The proposed algorithm delivers competitive inference speeds alongside other state-of-the-art methods. Notably, it achieves the lowest prediction time among all deep learning-based approaches, highlighting the efficiency of its multi-resolution architecture and layer design. Together, Tables 6 through 11 demonstrate that the proposed algorithm matches leading methods in performance while maintaining comparable computational efficiency.

Table 11: Average implementation time for the 250 test images

Algorithm	He [19]	Zhu [17]	Kim [38]	Cai [48]	Chen [52]	Li [62]	Proposed
Time (ms)	2955.6	18.7035	81.5504	712.0637	430.0656	270.2500	266.2095

3-3- Qualitative Comparison and real world applications

This section provides a visual quality comparison between the proposed method and several state-of-the-art algorithms. Figure 5-(a) displays a synthetic hazy test image, alongside the dehazed results produced by different methods. As illustrated in Fig. 5, the algorithms presented in [38] and [62] alter the color balance, introducing an unnatural green tint to the bottom region of the image. The methods in [17] and [19] produce overly bright outputs that lack natural appearance, while the approach in [52] results in darker areas—most notably in the top-left corner around the lamp. Comparing the outputs of [48] and the proposed method against the ground truth reveals that both retain some residual fog; however, the proposed method more effectively reduces the fog, resulting in a clearer and more realistic image.

Figure 5: Foggy image and the defogged one obtained by the proposed and conventional methods.

Fig. 6 presents another test sample for evaluation. As observed in Fig. 6-(g), details such as the prices on the yellow strip are diminished when processed using the algorithm in [62]. The approach in [38] compromises color fidelity, while the methods in [17], [19] and [52] produce visually striking yet unrealistic

colors. The method in [48] retains some fog in the output, whereas the proposed approach generates results most closely resembling the ground truth.

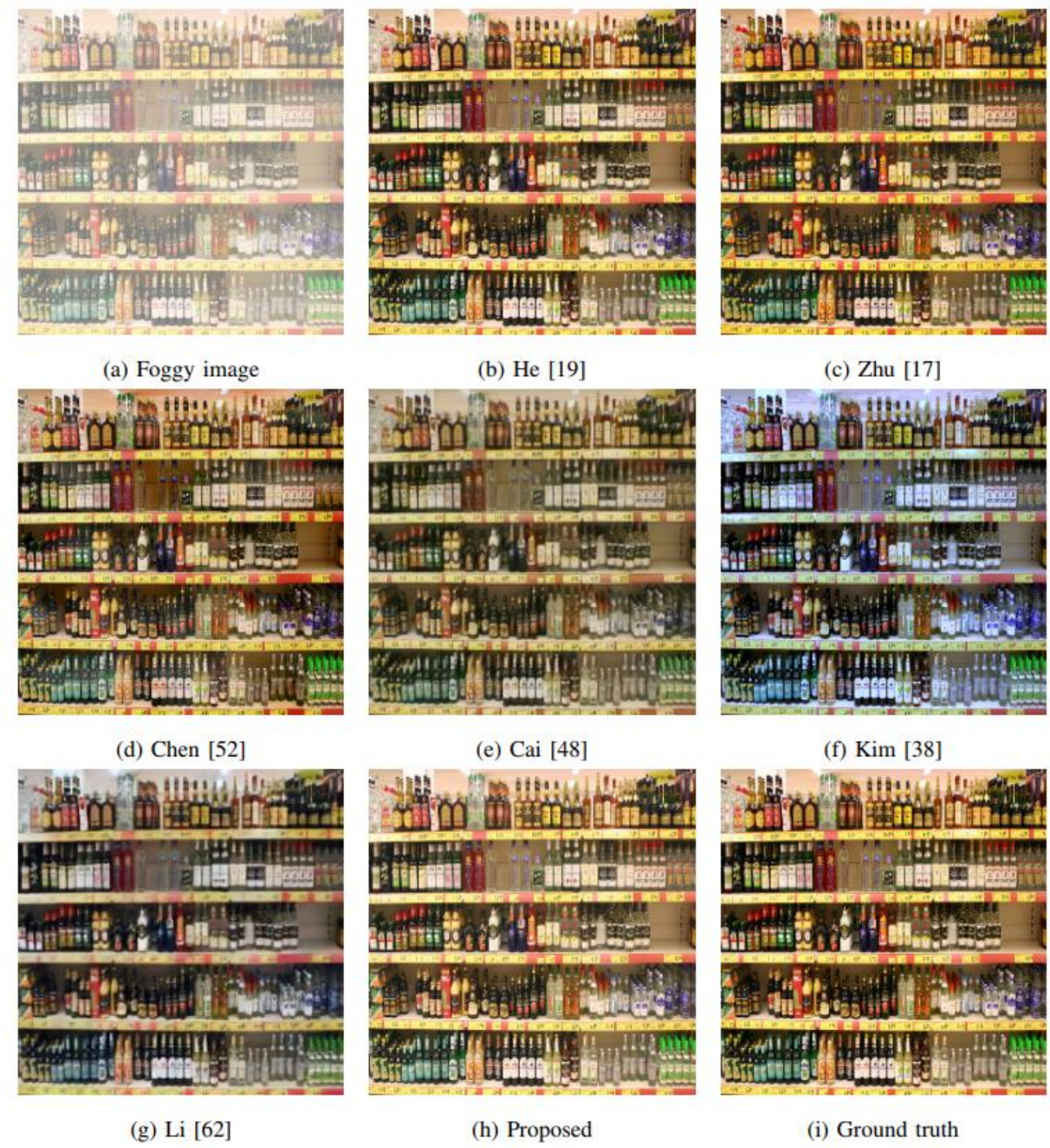

Figure 6: Foggy image and the defogged one obtained by the proposed and conventional methods.

Fig. 7 presents another test sample captured in an enclosed daylight environment. Upon closer inspection of the roof, artifacts are visible in the results from [38]. Additionally, the algorithms in [19], [17], and [52]

produce excessively bright colors, while the method in [62] introduces blurred colors and edges. Residual fog persists in the output of [48]. In contrast, the proposed method achieves colors that more closely match the ground truth, demonstrating superior fidelity.

Figure 7: Foggy image and the defogged one obtained by the proposed and conventional methods

Fig. 8 presents a real-world example illustrating the application of dehazing techniques. As observed in the figure, the algorithms in [38] and [62] exhibit poor color fidelity, resulting in unrealistic outputs. To further evaluate the visual quality of the proposed method, a user study was conducted. A total of 30 participants—20 men and 10 women—were shown pairs of hazy and ground truth images from the D-HAZE dataset, along with the corresponding dehazed results from seven different algorithms. Participants were asked to select the version they found most natural in appearance. The results of this subjective evaluation are summarized in Table 12, which shows that the majority of participants preferred the output generated by the proposed method. This indicates that the proposed algorithm produces more natural and realistic dehazing results compared to existing approaches.

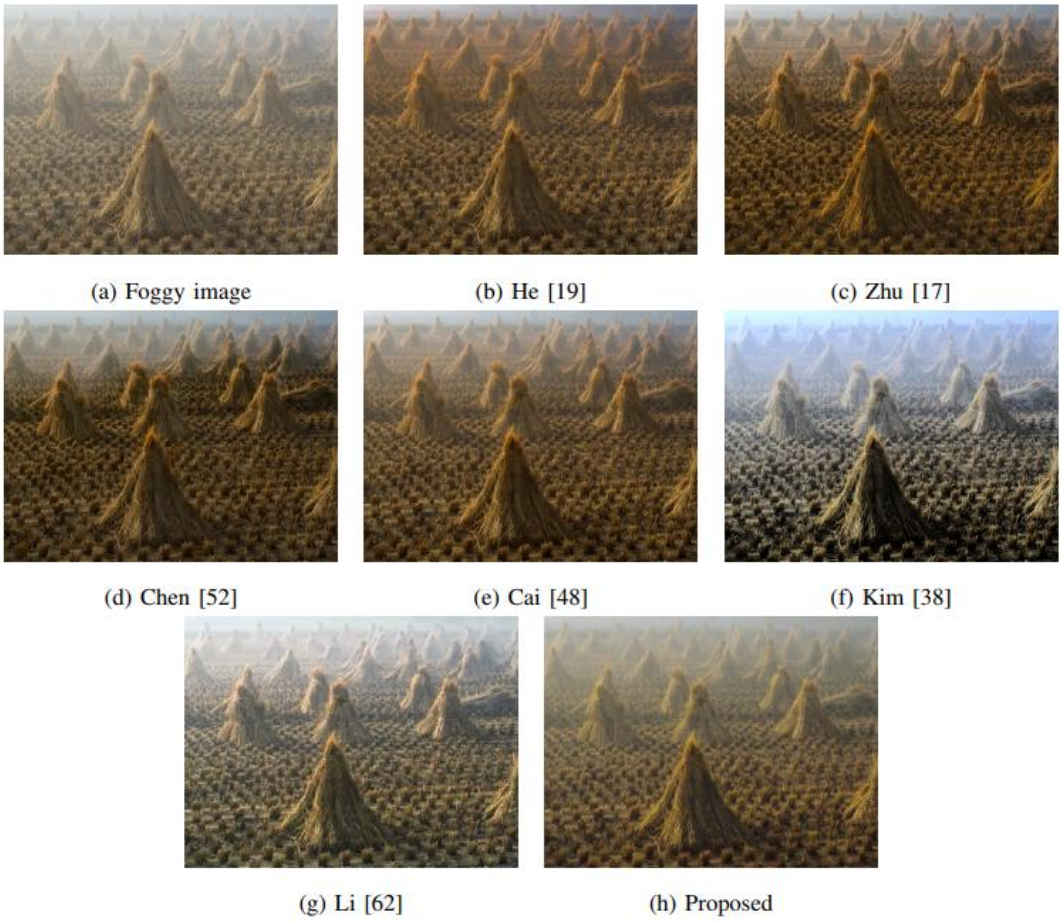

Figure 8: Foggy image and the defogged one obtained by the proposed and conventional methods.

Table 12: Real experiment from 30 persons including 20 men and 10 women.

Algorithm	He [19]	Zhu [17]	Kim [38]	Cai [48]	Chen [52]	Li [62]	Proposed
Votes	7	5	0	3	3	0	12

Fig. 9 compares the results of the proposed method with state-of-the-art algorithms on real foggy images. As shown, the proposed method recovers more details in the dehazed images compared with the other approaches. Tables 13 and 14 report the FADE and NIQE values for each sample, respectively. These tables indicate that the proposed method achieves the lowest FADE and NIQE scores in most cases, resulting in the best overall averages. Lower FADE and NIQE values demonstrate that the proposed algorithm delivers superior visual quality.

Synthetic foggy images were used because their corresponding clear images are available, enabling the computation of reference-based metrics such as SSIM and PSNR. Nevertheless, we also include Fig. 9 and Tables 13 and 14 to evaluate the proposed method on real foggy images. As shown in these results, the proposed approach consistently outperforms existing methods in most scenarios. Therefore, the findings of this study are reliable and generalizable to real foggy conditions.

3-4- Ablation study

To evaluate the effectiveness of the proposed architecture, this section analyzes the impact of its key components on overall network performance. Specifically, we compare the full model with two simplified variants: (a) a version in which the multi-level channel attention block is modified by removing the concatenation layer, and (b) a version without the low-level feature attention mechanism—i.e., the final element-wise multiplication shown in Fig. 2 is omitted, aslo, without the direct connection from the input to the output. This comparison highlights the contribution of each component to the network's performance. Fig. 10 demonstrates that the proposed method's variant without multi-level attention produces an unnaturally dark output. The exclusion of low-level attention similarly degrades performance, manifesting

10.22060/EEJ.2026.24359.5691

as both blurring artifacts and compromised color accuracy. In contrast, the complete proposed architecture achieves optimal results, validating the importance of its integrated attention mechanisms.

Table 13: FADE related to the restored image.

Algorithm	school bus	sweden	tiananmen	towers	canon	train
Cai [48]	1.9721	1.7295	1.6728	**1.171**	2.5756	1.4129
Fattal [14]	**0.61712**	2.2024	3.3949	2.1631	1.5873	2.2978
He [19]	2.2666	1.576	1.7223	1.978	2.0859	1.8239
Kim [38]	1.9961	1.3553	1.8917	1.6668	1.7355	1.3212
Mao [13]	1.3136	1.1127	1.3879	1.2702	1.6282	1.2768
He [20]	1.6097	1.2121	1.5375	1.4371	1.6891	1.3306
Tufail [21]	2.4556	1.6273	1.3755	1.4285	2.6433	2.2167
Yang [35]	1.6503	1.2912	1.5484	1.5248	1.8524	1.4457
Wen [24]	1.4304	1.1379	1.3071	1.3587	1.6155	1.2537
Tan [18]	1.3449	1.13	1.5646	1.3215	1.527	1.0717
Tarel [32]	2.0356	1.8126	1.3332	1.5016	2.2326	1.9604
Liu [10]	3.8908	3.8108	1.4353	1.5107	4.3705	3.0945
Ancuti [9]	2.8845	2.8056	2.3892	3.2097	3.0526	2.9672
Song [61]	1.3273	1.1243	1.4075	1.285	1.6548	1.2795
Li [62]	3.7223	3.035	4.338	3.9948	3.7313	3.4871
Zhu [17]	2.1835	2.0823	3.1428	2.0091	4.1885	1.2921
Yang [47]	2.6383	1.5623	1.9278	2.548	2.8521	1.678
Noori [41]	1.6278	1.1241	1.3959	1.5492	1.6790	1.3906
Chen [52]	1.7138	1.4617	1.9168	1.9218	1.842	1.4319
Ling [39]	2.6768	2.8143	2.2992	2.646	2.4416	**1.0431**
Chen [63]	4.326	3.2809	4.0943	4.7173	4.0721	4.2107
Proposed	1.1500	**1.0455**	**1.2895**	1.1953	**1.4761**	1.1158

10.22060/EEJ.2026.24359.5691

Table 15 reveals that the proposed method's variant lacking low-level attention underperforms compared to the version without multi-level attention. This finding underscores that optimal performance requires effective integration of extracted features rather than reliance on low-level features alone.

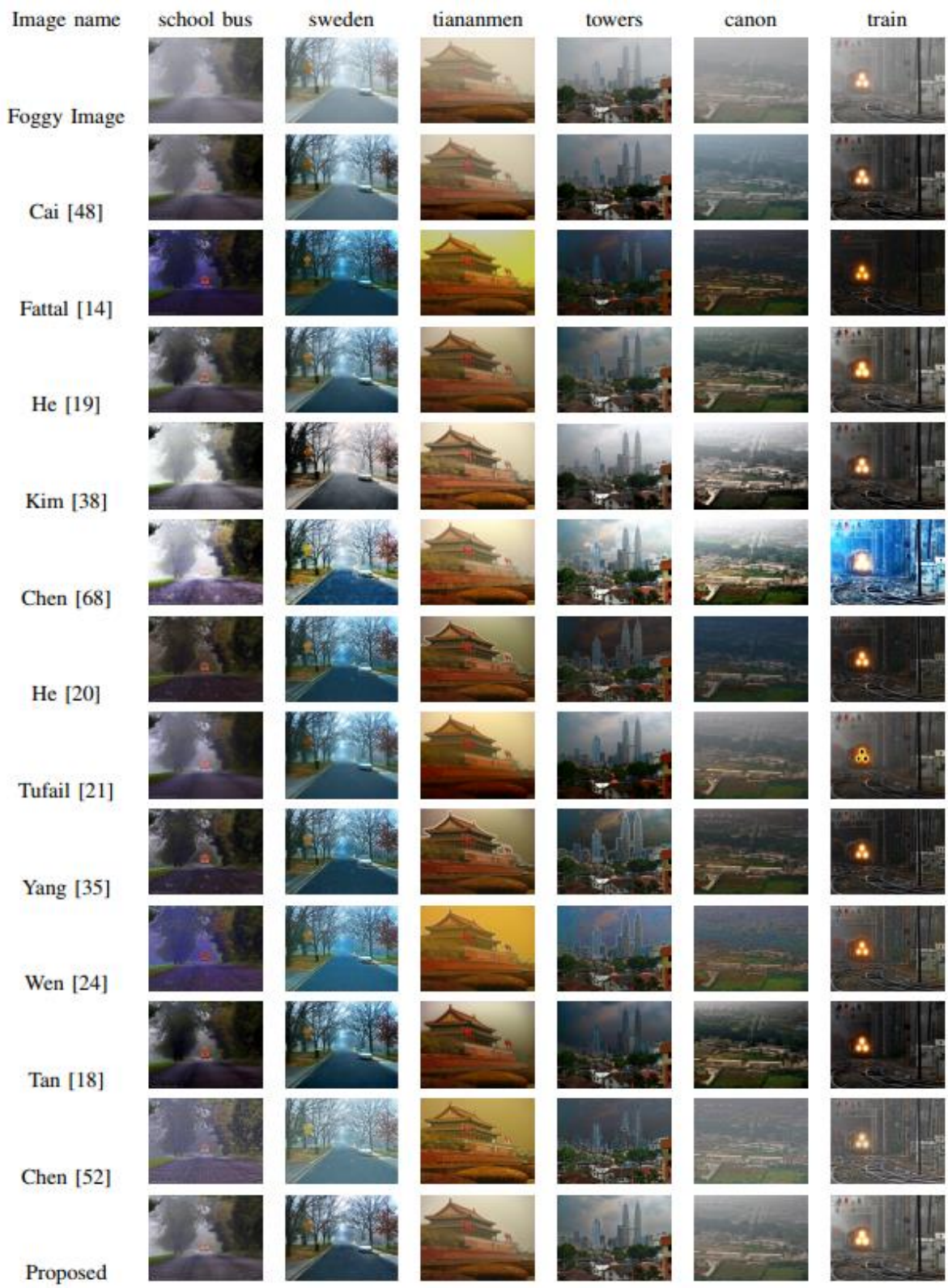

Figure 9: Foggy image and the defogged one obtained by the proposed and conventional methods.

Table 14: NIQE related to the restored image.

Algorithm	school bus	sweden	tiananmen	towers	canon	train
Cai [48]	2.3922	2.1518	3.2988	2.151	2.6511	2.9918
Fattal [14]	7.4202	1.8773	**2.1563**	2.5906	2.7769	4.3781
He [19]	3.3223	2.1839	3.1152	1.8575	2.7163	2.9021
Kim [38]	2.3853	3.0067	3.4936	2.8548	3.0493	3.1762
Mao [13]	4.2251	5.0559	3.2863	3.9245	3.8354	4.2967
He [20]	2.9695	3.0733	3.4699	2.5312	3.2102	3.9782
Tufail [21]	2.4834	3.137	3.4036	2.2253	2.7899	3.1197
Yang [35]	2.6375	2.4504	3.1011	2.2162	2.7977	3.0633
Wen [24]	5.1041	4.6538	4.0397	3.0911	5.7174	5.6451
Tan [18]	2.9874	2.5565	3.0011	2.5377	2.7047	2.8955
Tarel [32]	3.2558	4.1457	3.6895	3.1985	3.7146	4.0121
Liu [10]	2.3426	2.2363	3.4753	2.7824	2.7749	3.2295
Ancuti [9]	3.0542	2.3823	3.0768	2.3869	2.9964	**2.8215**
Song [61]	3.9961	4.8758	3.4039	3.7496	3.8676	4.4593
Li [62]	2.9662	2.8873	3.0363	2.6635	2.5868	3.5692
Zhu [17]	2.3669	2.3444	3.3179	1.9799	2.6696	3.3829
Yang [47]	2.5768	3.6863	3.0996	1.9738	3.0872	3.269
Noori [41]	2.3671	2.2091	3.1211	1.903	2.6742	3.011
Chen [52]	2.5560	2.2903	3.6271	2.4511	2.8790	3.4120
Ling [39]	2.7579	2.2098	3.1496	2.0109	2.8545	**2.7891**
Chen [63]	3.0355	3.8254	3.2187	3.9012	3.1211	3.008
Proposed	**2.1823**	**1.6941**	2.9939	**1.7655**	**2.4127**	2.6511

Additionally, a comparison of Table 15 with Tables 6 and 7 demonstrates that removing any block from the proposed method leads to a significant decline in performance, even relative to state-of-the-art

algorithms. This underscores the effectiveness of the proposed multi-level and low-level feature attention blocks.

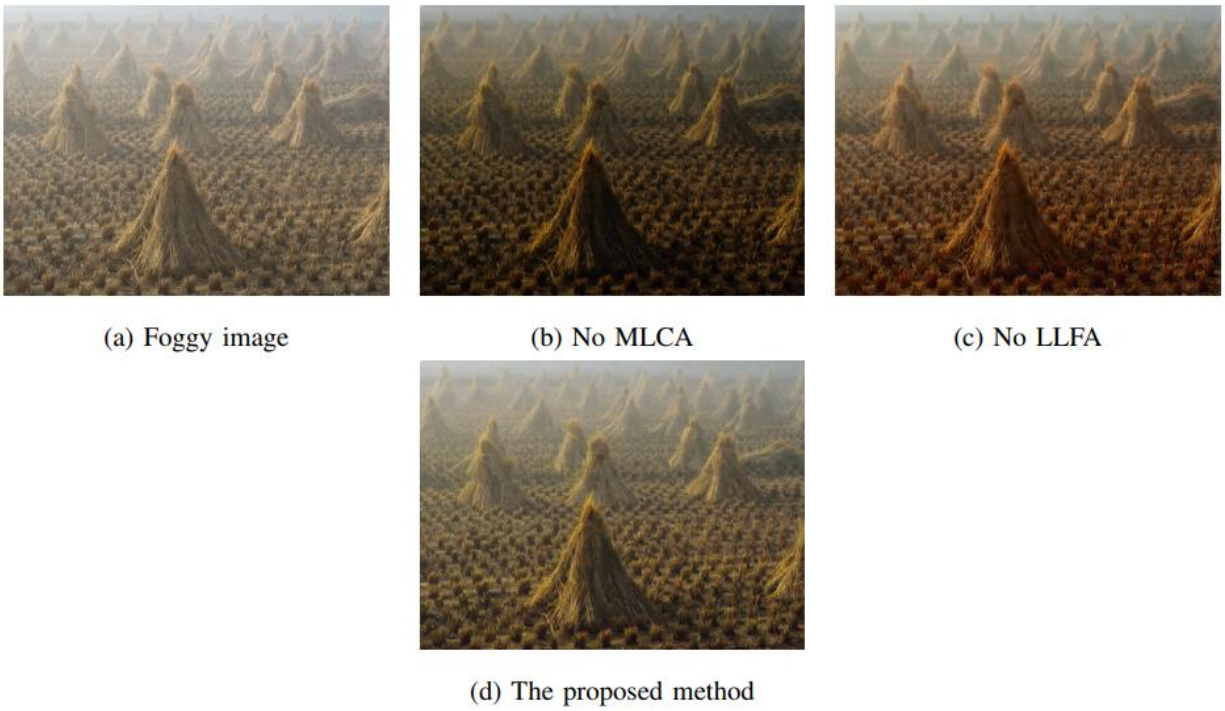

(a) Foggy image (b) No MLCA (c) No LLFA

(d) The proposed method

Figure 10: Foggy image and the defogged one obtained by different versions of the proposed method

Table 15: Comparing PSNR and SSIM for different versions of the proposed architecture

Algorithm	No MLCA	No LLFA	Proposed
PSNR	18.9072	18.8401	20.615
SSIM	0.8225	0.7431	0.9679

The impact of the number of MLCA blocks is illustrated in Figs. 11 and 12. As these figures show, both PSNR and SSIM increase as the number of MLCA modules increases, reaching their peak at 10 modules, after which the performance declines. Therefore, in this paper, 10 MLCA modules are used in each LLFA module.

10.22060/EEJ.2026.24359.5691

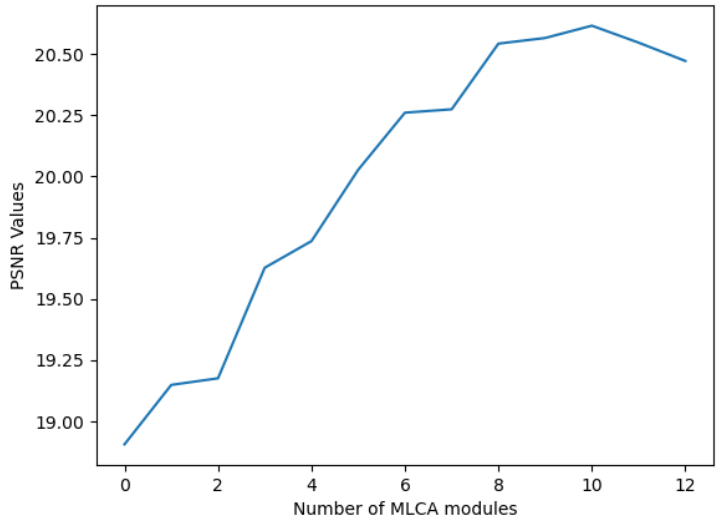

Figure 11: Obtained PSNR in terms of number of MLCA Modules used in the proposed architecture

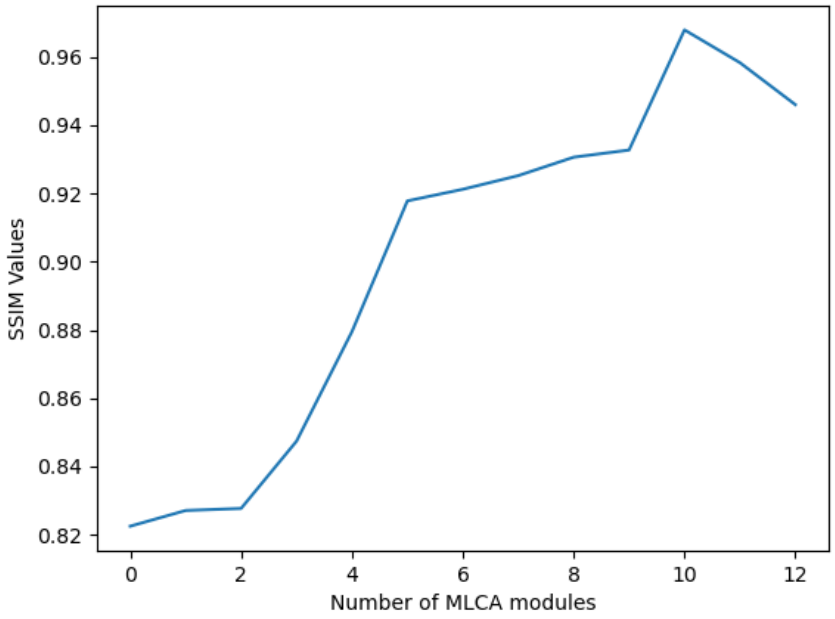

Figure 12: Obtained SSIM in terms of number of MLCA Modules used in the proposed architecture

As shown in Fig. 2, the LLFA module increases computational complexity only by performing a 128×128 elementwise matrix multiplication (i.e., 16,384 scalar multiplications). This is because the LLFA block simply connects low-level features to high-level features through elementwise operations. Similarly,

although the MLCA module concatenates features extracted from different convolutional layers, the channel attention module that follows performs global averaging across all concatenated channels and reduces them to a single channel. Thus, the MLCA module adds computational cost proportional to the number of concatenated channels multiplied by an elementwise matrix operation. Overall, both the LLFA and MLCA modules introduce only a modest increase in computational complexity.

4- Conclusion

This paper presents a novel architecture for single image dehazing, incorporating two key modules: Low-Level Feature Attention (LLFA) and Multi-Level Channel Attention (MLCA). The LLFA module is designed to preserve the contribution of low-level features, which are often diminished in deep networks, while the MLCA module effectively integrates both low- and high-level features to enhance the extraction of informative representations. These modules are applied across multiple resolutions to capture spatial dependencies across different regions of the image. Extensive comparisons with recent state-of-the-art algorithms demonstrate that the proposed architecture achieves superior performance in both qualitative and quantitative evaluations, confirming its effectiveness in restoring visibility and preserving image details in hazy conditions.

References:

[1] Z. Chen, Y. Wang, Y. Yang, D. Liu, PSD: Principled synthetic-to-real dehazing guided by physical priors, in: Proceedings of the IEEE/CVF conference on computer vision and pattern recognition, 2021, pp. 7180-7189.
[2] Y.Y. Schechner, S.G. Narasimhan, S.K. Nayar, Instant dehazing of images using polarization, in: Proceedings of the 2001 IEEE Computer Society Conference on Computer Vision and Pattern Recognition. CVPR 2001, IEEE, 2001, pp. I-I.
[3] Y.Y. Schechner, S.G. Narasimhan, S.K. Nayar, Polarization-based vision through haze, Applied optics, 42(3) (2003) 511-525.
[4] S.G. Narasimhan, S.K. Nayar, Chromatic framework for vision in bad weather, in: Proceedings IEEE Conference on Computer Vision and Pattern Recognition. CVPR 2000 (Cat. No. PR00662), IEEE, 2000, pp. 598-605.
[5] S.K. Nayar, S.G. Narasimhan, Vision in bad weather, in: Proceedings of the seventh IEEE international conference on computer vision, IEEE, 1999, pp. 820-827.
[6] C.O. Ancuti, C. Ancuti, Single image dehazing by multi-scale fusion, IEEE Transactions on Image Processing, 22(8) (2013) 3271-3282.

[7] J.-M. Guo, J.-y. Syue, V.R. Radzicki, H. Lee, An efficient fusion-based defogging, IEEE Transactions on Image Processing, 26(9) (2017) 4217-4228.
[8] A. Galdran, Image dehazing by artificial multiple-exposure image fusion, Signal Processing, 149 (2018) 135-147.
[9] C. Ancuti, C.O. Ancuti, C. De Vleeschouwer, A.C. Bovik, Day and night-time dehazing by local airlight estimation, IEEE Transactions on Image Processing, 29 (2020) 6264-6275.
[10] X. Liu, H. Li, C. Zhu, Joint contrast enhancement and exposure fusion for real-world image dehazing, IEEE transactions on multimedia, 24 (2021) 3934-3946.
[11] P. Pandey, R. Gupta, N. Goel, Enhancement of single foggy image using feature based fusion technique, Multimedia Tools and Applications, 84(23) (2025) 27401-27424.
[12] Y.-K. Wang, C.-T. Fan, Single image defogging by multiscale depth fusion, IEEE Transactions on image processing, 23(11) (2014) 4826-4837.
[13] W. Mao, D. Zheng, M. Chen, J. Chen, Single image defogging via multi-exposure image fusion and detail enhancement, Journal of Safety Science and Resilience, 5(1) (2024) 37-46.
[14] R. Fattal, Single image dehazing, ACM transactions on graphics (TOG), 27(3) (2008) 1-9.
[15] R. Fattal, Dehazing using color-lines, ACM transactions on graphics (TOG), 34(1) (2014) 1-14.
[16] D. Berman, S. Avidan, Non-local image dehazing, in: Proceedings of the IEEE conference on computer vision and pattern recognition, 2016, pp. 1674-1682.
[17] Q. Zhu, J. Mai, L. Shao, A fast single image haze removal algorithm using color attenuation prior, IEEE transactions on image processing, 24(11) (2015) 3522-3533.
[18] R.T. Tan, Visibility in bad weather from a single image, in: 2008 IEEE conference on computer vision and pattern recognition, IEEE, 2008, pp. 1-8.
[19] K. He, J. Sun, X. Tang, Single image haze removal using dark channel prior, IEEE transactions on pattern analysis and machine intelligence, 33(12) (2010) 2341-2353.
[20] X. He, J. Mao, Z. Liu, J. Zhou, Y. Hua, A fast algorithm for image defogging, in: Chinese Conference on Pattern Recognition, Springer, 2014, pp. 149-158.
[21] Z. Tufail, K. Khurshid, A. Salman, I.F. Nizami, K. Khurshid, B. Jeon, Improved dark channel prior for image defogging using RGB and YCbCr color space, IEEE Access, 6 (2018) 32576-32587.
[22] A. Kumari, S. Sahdev, S. Sahoo, Improved single image and video dehazing using morphological operation, in: 2015 International Conference on VLSI Systems, Architecture, Technology and Applications (VLSI-SATA), IEEE, 2015, pp. 1-5.
[23] K. He, J. Sun, X. Tang, Guided image filtering, IEEE transactions on pattern analysis and machine intelligence, 35(6) (2012) 1397-1409.
[24] S. Wen, Y. Zhao, J. Ma, H. keung Lam, H. Wang, Image defogging algorithm based on image bright and dark channels, in: 2018 WRC Symposium on Advanced Robotics and Automation (WRC SARA), IEEE, 2018, pp. 269-274.
[25] C. Zhen, S. Jihong, P. Roth, Single Image Defogging Algorithm based on Dark Channel Priority, Journal of Multimedia, 8(4) (2013).
[26] Z. Tufail, K. Khurshid, A. Salman, K. Khurshid, Optimisation of transmission map for improved image defogging, IET Image Processing, 13(7) (2019) 1161-1169.
[27] F. Guo, H. Peng, J. Tang, A new restoration algorithm for single image defogging, in: Chinese Conference on Pattern Recognition, Springer, 2014, pp. 169-178.
[28] R.M. Yousaf, H.A. Habib, Z. Mehmood, A. Banjar, R. Alharbey, O. Aboulola, Single Image Dehazing and Edge Preservation Based on the Dark Channel Probability-Weighted Moments, Mathematical Problems in Engineering, 2019(1) (2019) 9721503.
[29] L. He, J. Zhao, N. Zheng, D. Bi, Haze removal using the difference-structure-preservation prior, IEEE transactions on image processing, 26(3) (2016) 1063-1075.

[30] M. Ju, D. Zhang, X. Wang, Single image dehazing via an improved atmospheric scattering model, The Visual Computer, 33(12) (2017) 1613-1625.
[31] I. Yoon, S. Kim, D. Kim, M.H. Hayes, J. Paik, Adaptive defogging with color correction in the HSV color space for consumer surveillance system, IEEE transactions on consumer electronics, 58(1) (2012) 111-116.
[32] J.-P. Tarel, N. Hautiere, Fast visibility restoration from a single color or gray level image, in: 2009 IEEE 12th international conference on computer vision, IEEE, 2009, pp. 2201-2208.
[33] A. Sabir, K. Khurshid, A. Salman, Segmentation-based image defogging using modified dark channel prior, EURASIP Journal on Image and Video Processing, 2020(1) (2020) 6.
[34] M.I. Anwar, A. Khosla, Vision enhancement through single image fog removal, Engineering science and technology, an international journal, 20(3) (2017) 1075-1083.
[35] F. Yang, Y. Hu, Improved Dark Channel Prior for Image Defogging, in: 2022 International Conference on Artificial Intelligence and Computer Information Technology (AICIT), IEEE, 2022, pp. 1-4.
[36] C. Qin, X. Gu, A single image dehazing method based on decomposition strategy, Journal of Systems Engineering and Electronics, 33(2) (2022) 279-293.
[37] X. Kang, Z. Fei, P. Duan, S. Li, Fog model-based hyperspectral image defogging, IEEE Transactions on Geoscience and Remote Sensing, 60 (2021) 1-12.
[38] S.E. Kim, T.H. Park, I.K. Eom, Fast single image dehazing using saturation based transmission map estimation, IEEE Transactions on Image Processing, 29 (2019) 1985-1998.
[39] P. Ling, H. Chen, X. Tan, Y. Jin, E. Chen, Single image dehazing using saturation line prior, IEEE Transactions on Image Processing, 32 (2023) 3238-3253.
[40] W. Zhang, L. Dong, X. Pan, J. Zhou, L. Qin, W. Xu, Single image defogging based on multi-channel convolutional MSRCR, IEEE Access, 7 (2019) 72492-72504.
[41] H. Noori, M.H. Gholizadeh, H.K. Rafsanjani, Digital image defogging using joint Retinex theory and independent component analysis, Computer Vision and Image Understanding, 245 (2024) 104033.
[42] J. Wang, K. Lu, J. Xue, N. He, L. Shao, Single image dehazing based on the physical model and MSRCR algorithm, IEEE Transactions on Circuits and Systems for Video Technology, 28(9) (2017) 2190-2199.
[43] G. Qingqing, W. Xiangping, W. Ke, W. Shuang, H. Shaowei, Adaptive Retinex image defogging algorithm based on the depth of field information, in: 2022 IEEE Intl Conf on Dependable, Autonomic and Secure Computing, Intl Conf on Pervasive Intelligence and Computing, Intl Conf on Cloud and Big Data Computing, Intl Conf on Cyber Science and Technology Congress (DASC/PiCom/CBDCom/CyberSciTech), IEEE, 2022, pp. 1-7.
[44] F. Guo, J. Yang, Z. Liu, J. Tang, Haze removal for single image: A comprehensive review, Neurocomputing, 537 (2023) 85-109.
[45] Y. Xu, J. Wen, L. Fei, Z. Zhang, Review of video and image defogging algorithms and related studies on image restoration and enhancement, Ieee Access, 4 (2015) 165-188.
[46] J. Wang, H. Wang, Y. Sun, J. Yang, Improved retinex-theory-based low-light image enhancement algorithm, Applied Sciences, 13(14) (2023) 8148.
[47] M. Yang, Z. Li, J. Liu, Super-pixel based single image haze removal, in: 2016 Chinese Control and Decision Conference (CCDC), IEEE, 2016, pp. 1965-1969.
[48] B. Cai, X. Xu, K. Jia, C. Qing, D. Tao, Dehazenet: An end-to-end system for single image haze removal, IEEE transactions on image processing, 25(11) (2016) 5187-5198.
[49] S. Yin, X. Yang, R. Lu, Z. Deng, Y.-H. Yang, Visual Attention and ODE-inspired Fusion Network for image dehazing, Engineering Applications of Artificial Intelligence, 130 (2024) 107692.
[50] B. Xiao, Z. Zheng, Y. Zhuang, C. Lyu, X. Jia, Single UHD image dehazing via interpretable pyramid network, Signal Processing, 214 (2024) 109225.
[51] B. Li, X. Peng, Z. Wang, J. Xu, D. Feng, Aod-net: All-in-one dehazing network, in: Proceedings of the IEEE international conference on computer vision, 2017, pp. 4770-4778.

[52] Z. Chen, Z. He, Z.-M. Lu, DEA-Net: Single image dehazing based on detail-enhanced convolution and content-guided attention, IEEE transactions on image processing, 33 (2024) 1002-1015.
[53] H. Zhang, V.M. Patel, Densely connected pyramid dehazing network, in: Proceedings of the IEEE conference on computer vision and pattern recognition, 2018, pp. 3194-3203.
[54] Z. Zheng, W. Ren, X. Cao, X. Hu, T. Wang, F. Song, X. Jia, Ultra-high-definition image dehazing via multi-guided bilateral learning, in: 2021 IEEE/CVF Conference on Computer Vision and Pattern Recognition (CVPR), IEEE, 2021, pp. 16180-16189.
[55] X. Qin, Z. Wang, Y. Bai, X. Xie, H. Jia, FFA-Net: Feature fusion attention network for single image dehazing, in: Proceedings of the AAAI conference on artificial intelligence, 2020, pp. 11908-11915.
[56] D. Chen, M. He, Q. Fan, J. Liao, L. Zhang, D. Hou, L. Yuan, G. Hua, Gated context aggregation network for image dehazing and deraining, in: 2019 IEEE winter conference on applications of computer vision (WACV), IEEE, 2019, pp. 1375-1383.
[57] X. Liu, Y. Ma, Z. Shi, J. Chen, Griddehazenet: Attention-based multi-scale network for image dehazing, in: Proceedings of the IEEE/CVF international conference on computer vision, 2019, pp. 7314-7323.
[58] Y. Qu, Y. Chen, J. Huang, Y. Xie, Enhanced pix2pix dehazing network, in: Proceedings of the IEEE/CVF conference on computer vision and pattern recognition, 2019, pp. 8160-8168.
[59] J. Ming, Z. Cai, S. Li, S. Bi, Y. Ning, Single image dehazing based on convolutional neural network and multiple attention fusion, Signal, Image and Video Processing, 19(4) (2025) 294.
[60] L. Lu, Q. Xiong, B. Xu, D. Chu, Mixdehazenet: Mix structure block for image dehazing network, in: 2024 International Joint Conference on Neural Networks (IJCNN), IEEE, 2024, pp. 1-10.
[61] Y. Song, Z. He, H. Qian, X. Du, Vision transformers for single image dehazing, IEEE Transactions on Image Processing, 32 (2023) 1927-1941.
[62] J. Li, Y. Li, L. Zhuo, L. Kuang, T. Yu, USID-Net: Unsupervised single image dehazing network via disentangled representations, IEEE transactions on multimedia, 25 (2022) 3587-3601.
[63] J. Chen, G. Zhao, Contrastive multiscale transformer for image dehazing, Sensors, 24(7) (2024) 2041.
[64] W. Li, D. Fan, Q. Zhu, Z. Gao, H. Sun, HEDehazeNet: Unpaired image dehazing via enhanced haze generation, Image and Vision Computing, 150 (2024) 105236.
[65] L.K. Choi, J. You, A.C. Bovik, Referenceless prediction of perceptual fog density and perceptual image defogging, IEEE Transactions on Image Processing, 24(11) (2015) 3888-3901.
[66] A. Mittal, R. Soundararajan, A.C. Bovik, Making a “completely blind” image quality analyzer, IEEE Signal processing letters, 20(3) (2012) 209-212.
[67] M. Yu, S. Xu, H. Sun, Y. Zheng, W. Yang, Hierarchical slice interaction and multi-layer cooperative decoding networks for remote sensing image dehazing, Image and Vision Computing, 148 (2024) 105129.
[68] B. Li, W. Ren, D. Fu, D. Tao, D. Feng, W. Zeng, Z. Wang, Benchmarking single-image dehazing and beyond, IEEE transactions on image processing, 28(1) (2018) 492-505.